Self-Alignment of Interference Arising From Hallway Guidance of Diffuse Fields

Dmitry Chizhik, *Fellow, IEEE*, Jonathan Ling, and Reinaldo A. Valenzuela, *Fellow, IEEE*

***Abstract*—Propagation theory is developed to get analytic expressions for both guided and diffusely scattered 3-D fields in common indoor environments, with access points (APs) placed along a hallway and mobile nodes in the rooms. Resulting predictions agree with measurements of both path loss and single-user multiple-input–multiple-output link capacity. In particular, the model reproduces the observed reduction in normalized channel capacity with increasing range. This effect, occurring in a common indoor environment, can be beneficial. Interfering APs, which tend to be further away, occupy channel dimensions corresponding to low-order hallway modes, causing total interference to concentrate in a small subset of the channel dimensions, in a manner reminiscent of interference alignment. The channel for the desired signal has a greater number of effective degrees of freedom (EDOFs) due to a shorter distance from its serving AP. The disparity in the number of EDOFs between the signal and the interference leads to higher rates, which can be further increased through waterfilling applied individually to each link, with no interlink coordination. The resulting rates are on the order of 30% greater than would be anticipated in range-independent scattering models.**

***Index Terms*—Diffusion, capacity, indoor environment, propagation loss, MIMO, waveguide.**

I. Introduction

In this work, we examine indoor radio propagation, its impact on single-user multiple-input–multiple-output (SU-MIMO) links as well as rates in a multi-cell indoor network. The goal of the propagation modeling here is to construct a canonical 3D propagation model based on limited information about the environment, yet faithful to retaining relevant physical effects.

Use of N_{T} transmit antennas and N_{R} receive antennas with MIMO techniques [1], [2] promises link capacity that scales as $\min(N_{\mathrm{R}}, N_{\mathrm{T}})$, provided the channel variation with time and frequency is gradual enough to allow the receiver to "learn" the channel with low overhead [3], [4]. This is usually satisfied, particularly in small cell, low-mobility cases.

Furthermore, two critical conditions for validity of such scaling are sufficiently rich scattering [2] and sufficiently high signal-to-interference-plus-noise ratio (SINR). Measurement campaigns, conducted both outdoors (e.g., [5]) and indoors (e.g., [6]), have reported scattering to be rich enough to offer capacities that are generally a large fraction of the capacity of the canonical independent identically distributed (i.i.d.) channel. This has led to standard model recommendations [7], [8] of high angle spread indoors, usually larger than 40°. However, it was found through measurements that the (spatial) Rician K-factor at the node placed in the corridor increased with range [8], implying a reduction in the effective degrees of freedom (EDOF), defined in [33].

When the channel state is known at the transmitter as well, still higher link rate may be achieved through the closed-loop MIMO technique [9], by driving the eigenmodes of the channel as effective antennas, each with power determined by waterfilling (WF). This may be contrasted with open-loop MIMO [1], which uses equal power distribution, with multiple spatial streams usually applied to physical antennas.

Intercell interference in mature networks is well-known to severely limit available SINR. In the presence of intercellular interference and conditions of nearly i.i.d. channels for both desired and interfering signals, effective use of SU-MIMO is limited to a relatively small fraction of users fortunate enough to enjoy unusually high SINR, usually at short range from the serving base station. Alternatively, when channel conditions and backhaul network allow for channel knowledge at the transmitter, multi-user MIMO (MU-MIMO) techniques are an effective use of multiple antennas. Key requirement is timely and detailed channel state feedback for all links in coordination area or, else, calibrated time-division duplexing (TDD) signaling. MU-MIMO and intercell coordination methods [11], are not considered here.

Indoor propagation has been analyzed through modeling hallways as waveguides in [20], [21], [25]. Waveguide losses were included through representing walls as lossy dielectric halfspaces, with wall roughness included as a source of mode coupling. Penetration into rooms was modeled as penetration from the hallway into a dielectric subspace. The predicted power agreed well with measurements in hallways. The agreement was also reasonably good in adjacent rooms when the hallway contained the transmitter. The theory predicted dramatically higher losses than observed in more distant rooms, particularly for rooms adjacent to hallways other than the one containing the transmitter. This was attributed to the oversimplified wall penetration model. The modal theory was successful in representing decay in measured MIMO capacity in hallways, reported in [22], [25].

In this work, the environment of a single hallway, lined with rooms, is considered, with the aim of constructing a canonical indoor model of complex channel responses in agreement with observed propagation losses and MIMO capacities, both in the

Manuscript received June 17, 2013; revised December 2, 2013 and March 3, 2014; accepted May 3, 2014. Date of current version July 8, 2014. The associate editor coordinating the review of this paper and approving it for publication was J. Wallace.

The authors are with the Wireless Communications Research Department, Bell Laboratories, Alcatel-Lucent, Holmdel, NJ 08904 USA (e-mail: dmitry.chizhik@alcatel-lucent.com).

Color versions of one or more of the figures in this paper are available online at http://ieeexplore.ieee.org.

Digital Object Identifier 10.1109/TWC.2014.2326160

hallway and in rooms. While hallway propagation is treated as a lossy waveguide, propagation into rooms is accounted for by representing room scattering as a diffusion process, reproducing well-documented rich scattering in rooms [25], important for MIMO. In Sections III–V, discussion and analysis of propagation through diffuse scattering, hallway guidance and penetration into rooms are presented, respectively. Predicted path loss and single link MIMO capacity are found to compare well against measurements in Sections VI and VII. In Section VIII, the model is used to compute user rates in a multicell indoor environment, with access points (APs) arranged in a line along a hallway, while mobile users are in rooms off the hallway, each assigned to its strongest AP. All APs and mobile units are equipped with multiple antennas. It is found that interfering APs are naturally aligned by hallway propagation to occupy a subspace of the total channel, leading to higher capacity than an i.i.d. channel model would suggest. This is an example of natural interference filtering that may be contrasted to intentional interference alignment [26], a technique that requires channel state information at all transmitters. Novel aspects include propagation modeling through coupling of diffuse and guided fields, and identification of the self-alignment of interference as the mechanism for improved system capacity.

II. Deterministic and Statistical Fields

Fields may be purely deterministic, purely diffuse, as well as "structured". The term "structured" describes fields that have some aspect affected by the environment in a biased (usually predictable) way, while still being non-deterministic. An example of this is a light (or radio) field emitted by a distant star. The extended effective source of this glowing body creates a random (complex Gaussian) field, and, when measured at a large distance, the field appears to originate from a point source of randomly fluctuating amplitude, with a great deal of local spatial coherence, i.e., structure, at the receiver. Propagation through interstellar space, here idealized as free space, thus imposes a spatial structure on the otherwise random field. Other examples of structuring include various forms of the "keyhole" channel [12], [13].

One may identify hallways as effective waveguides that provide a relatively low path loss from the transmitter to the receiver and affect coherence properties of the field. Here, the indoor environment being considered is that of a hallway, lined with rooms on both sides, as illustrated in Fig. 1. Key aspects of propagation in a waveguide is that the solution is a superposition of modes, each mode being excited, propagated (i.e., undergoing a phase shift and attenuation), and then received. Since the modes are a property of the waveguide, signals from all sources are conveyed on the same set of modes. Presence of many modes of comparable strength implies a potential for rich scattering, while presence of few modes (say due to attenuation) implies poor scattering. In the extreme but illustrative case of a single mode, signals from all sources are confined to that mode, and the channel is seen as having a single degree of freedom. All sources are thus "aligned" on a single degree of freedom.

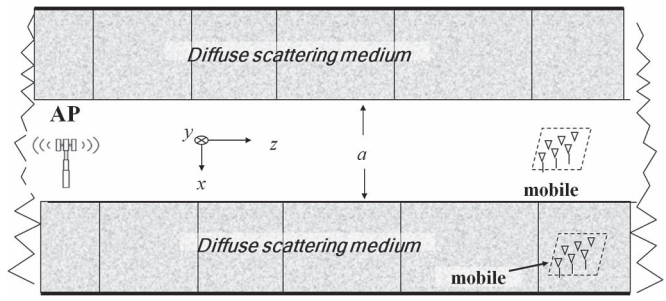

Fig. 1. Indoor environment (top view) with AP placed in the hallway and mobiles placed either in the hallway or in a (clutter-filled) room.

III. Diffusely Scattered Field

Unstructured scattering from furniture and other clutter (as opposed to, say, hallway walls) may be described using the diffuse scattering theory. Using the solution to the diffusion approximation of the radiative transfer problem in homogeneous media [14], the complex field $U_{\rm diff}(\mathbf{r})$ at location $\mathbf{r}$ due to a source at the origin is given by [14]:

$$U_{\rm diff}(\mathbf{r}) = \frac{e^{-\kappa r/2}}{4\pi}\sqrt{\kappa/r + 1/r^2}\,\xi_{\rm u}(\mathbf{r}). \tag{1}$$

Here, κ is the effective absorptive loss ($\kappa = 0.18$ nepers/m was found as fitting general non-line-of-sight (NLOS) indoor measurements best [16]) and i.i.d. $\xi_{\rm u}(\mathbf{r}) \sim \mathcal{CN}(0,1)$, denoting zero mean, unit variance complex Gaussian distributed field. Note that $U_{\rm diff}$ in (1) is a complex field, while [14] (and [16]) denotes the average intensity as U. The spatially white nature of (1) accounts for the fields impinging from all directions at the receiver, and is consistent with the rich scattering implied by the diffusion conditions. For spherically symmetrical spatial spectra consistent with the diffusion assumption, spatial structure is expressed [17] by field correlation as follows:

$$\langle \xi_{\rm u}(\mathbf{r})\xi_{\rm u}^*(\mathbf{r}')\rangle = j_0\left(k|\mathbf{r}-\mathbf{r}'|\right). \tag{2}$$

The notation $\langle\rangle$ indicates the expected value, $j_0(x) = \sin x/x$ is the spherical Bessel function and $k = 2\pi/\lambda$ is the wavenumber, defined in terms of the wavelength q. When the angular spectrum and $\mathbf{r}-\mathbf{r}'$ are confined to the same plane, the correlation is given by a cylindrical Bessel function $J_0(k|\mathbf{r}-\mathbf{r}'|)$. The correlation (2) takes significant values $j_0(x) \approx 1$ for $x < 1$ and, for the important case of antennas separated by at least $\lambda/2$, is, thus

$$\langle \xi_{\rm u}(\mathbf{r})\xi_{\rm u}^*(\mathbf{r}')\rangle \approx 0, |\mathbf{r}-\mathbf{r}'| < \lambda/2. \tag{3}$$

Use of the diffusion approximation to the transport equation for indoor radio modeling was first suggested by Ullmo and Baranger [15], who have reported that a 2D solution represented the data well for ranges over 15 m. In [16], it was found that a full 3D solution (1) represents the measurements well for all ranges, when the receiver and the transmitter are, in general, NLOS conditions.

IV. Propagation in a Hallway Waveguide

Signals received in a hallway due to a source also in the hallway are evaluated through modeling the hallway as a lossy waveguide, with width a along x and height b along y, as illustrated in Fig. 1. The walls are considered as a stack of dielectric layers, which, for the dominant low order modes, are approximated here as a Dirichlet (zero field) boundary for both polarizations. Field at $\mathbf{r} = (x, y, z)$ due to a point source at $\mathbf{r}_s = (x_s, y_s, z_s)$ in a waveguide forms the definition of the Green's function $G(\mathbf{r}, \mathbf{r}_s)$, here represented as a sum of modes. Each mode describes a two-dimensional field distribution across the $x - y$ cross-section of the waveguide and is indexed by an index pair m, n. The field of a point source is then

$$G(\mathbf{r}, \mathbf{r}_s) = \sum_{m,n} \psi_{mn}(x, y)\psi_{mn}(x_s, y_s) \times \frac{e^{i\beta_{mn}|z-z_s|} L_{mn}(z - z_s)}{2i\beta_{mn}}, \quad (4)$$

where the mnth mode is modified from the traditional conducting waveguide in [18], [19] as follows:

$$\psi_{mn}(x, y) = \frac{2}{\sqrt{ab}} \sin(m\pi x/a) \sin(n\pi y/b). \quad (5)$$

Still more accurate consideration of the dielectric wall properties [20] shows only a small correction to the above formulation, which is neglected here. It should be noted that the more accurate formulation becomes more significant for wall-mounted antennas. The scalar field (4) may be viewed [23] as the appropriate component of the Hertz potential, from which the electric and magnetic fields may be derived. The modal propagation constant β_{mn}(along z) is defined in terms of the wavenumber $k = 2\pi/\lambda$ for wavelength λ:

$$\beta_{mn} = \sqrt{k^2 - (m\pi/a)^2 - (n\pi/b)^2}. \quad (6)$$

Here, only propagating modes were included, thus m, $n \in [1, 2, \ldots]$, s.t. $\mathrm{Im}\beta_{mn} = 0$. At 2 GHz, for the hallway considered here, of width $a = 1.65$ m and height $b = 3$ m, the total number of propagating modes is about 650, easily within reach of modern computers to evaluate (4). At most ranges of interest, a smaller subset of only lower-order modes is sufficient [20]. The modal loss L_{mn} is derived in Appendix A. The form (5) of the mode functions is such that in the limit of an infinitely high and an infinitely wide waveguide, (4) reproduces 2-ray propagation behavior (at finite distance from the ground plane), including the $1/\mathrm{z}^4$ power decay with range z, well documented for both polarizations [34].

The complete Green's function in the actual hallway should account for penetration into dielectric walls as well as subsequent scattering from furniture and structures beyond the hallway walls. To keep the theoretical treatment tractable, we idealize this through a perturbation approach where the modal functional form (5) is preserved, but loss due to wall penetration is accounted for by the factor L_{mn}, derived in Appendix A from per-bounce loss experienced by the plane-wave representation of the mode functions. In the case of interior walls (as opposed to concrete), the "loss" experienced by each mode is mostly coupled to propagation external to the hallway. Most of that energy undergoes multiple scattering which includes absorption in concrete floors. Parts of those fields that are coupled back into the hallway are neglected here. The approximation used here preserves the mode shapes derived for a lossless guide, resulting in zero field at the side walls. This holds best for low-order modes, characterized by glancing incidence at walls and weak penetration into rooms. Fields associated with high-order modes may have higher amplitudes near walls, but are diminished by larger propagation "losses" L_{mn}. Mode coupling through wall roughness [20] is neglected here. Since the modal attenuation coefficient L_{mn} in (4) is based on the plane wave reflection coefficient, polarization-dependent effects, such as greater wall "losses" due to Brewster angle effect may be included, although only vertical polarization results are discussed here. For small (dipole) source and receive antennas, both placed in the same hallway, the field is well approximated by the Green's function (4):

$$U(\mathbf{r}, \mathbf{r}_s) = G(\mathbf{r}, \mathbf{r}_s). \quad (7)$$

V. Penetration Into Rooms

In this section, NLOS propagation between a hallway transmitter and a receiver placed in a room is modeled by representing the room environment as a diffusely scattering medium, whose (random) field is coupled to the hallway waveguide modes, resulting in a stochastic model of the complex field whose statistical structure is affected by hallway propagation. It is convenient to rely on reciprocity and regard the remote as the source, with a hallway AP as a receiver. When the remote location $\mathbf{r}$ is in a room adjacent to the hallway, Huygen's principle may be used to compute the field $U(\mathbf{r}, \mathbf{r}_s)$ at a hallway location $\mathbf{r}_s$, based on the field $U(\mathbf{r}, \mathbf{r}')$ and its gradient $\nabla' U(\mathbf{r}, \mathbf{r}')$ acting as secondary sources at intermediate locations $\mathbf{r}'$:

$$U(\mathbf{r}, \mathbf{r}_s) = \int\int d\mathbf{A}' \cdot \left(U(\mathbf{r}, \mathbf{r}')\nabla' G(\mathbf{r}', \mathbf{r}_s) - G(\mathbf{r}', \mathbf{r}_s)\nabla' U(\mathbf{r}, \mathbf{r}')\right). \quad (8)$$

In the surface integral on the right-hand side of (8), $d\mathbf{A}'$ is the elemental area, field $U(\mathbf{r}, \mathbf{r}')$ is the field at intermediate point $\mathbf{r}'$ due to source at $\mathbf{r}$ outside the hallway, and $G(\mathbf{r}', \mathbf{r}_s)$ is the hallway Green's function (4). The area integration and the gradient operator ∇' are defined over the (intermediate) primed coordinates $\mathbf{r}'$. Subscript s for coordinates of a hallway receiver is retained for notational consistency with Section IV. The integration is over an area enclosing the source. It is convenient to use the relatively simple form of the Green's function (4), valid in the hallway, so hallway walls are chosen as the integration boundary. As an approximation, only the wall along the side of the hallway adjacent to the room is selected, where the effective source field is strongest. The problem has thus been transformed into a problem where there is a distributed equivalent source, namely, a "hot" wall (illuminated by a field launched from a source inside a room in diffuse scattering conditions). The received field in the hallway waveguide is

given by the superposition integral (8), simplified by recognizing that the Green's function (4) is zero at the integration surface and its gradient is parallel to x (i.e., orthogonal to the "hot" wall):

$$U(\mathbf{r},\mathbf{r}_s)=\int_{-b/2}^{b/2}dy'\int_{-\infty}^{\infty}dz'U(\mathbf{r}',\mathbf{r})\frac{\partial G(\mathbf{r}',\mathbf{r}_s)}{\partial x'}\bigg|_{x'=0}. \quad (9)$$

Using (4) and (5)

$$\frac{\partial G}{\partial x'}\bigg|_{x'=0}=\sum_{m,n}\frac{2}{\sqrt{ab}}\sin\left(\frac{n\pi y'}{b}\right)\psi_{mn}(x_s,y_s)\times\frac{m\pi e^{i\beta_{mn}|z'-z_s|}L_{mn}}{2ai\beta_{mn}} \quad (10)$$

and integrating, (9) may be re-written as a modal sum

$$U(\mathbf{r},\mathbf{r}_s)=\sum_{m,n}\frac{1}{2i\beta_{mn}}\psi_{mn}(x_s,y_s)E_{mn}(\mathbf{r},\mathbf{r}_s). \quad (11)$$

As discussed in Appendix B, the modal coupling coefficient E_{mn} consists of guided and direct components (B-12), allowing the decomposition of (11):

$$U=U^{\mathrm{g}}+U^{\mathrm{d}}. \quad (12)$$

$$U^{\mathrm{g}}(\mathbf{r},\mathbf{r}_s)=\sum_{m,n}\frac{1}{2i\beta_{mn}}\psi_{mn}(x_s,y_s)E^{\mathrm{g}}_{mn}(\mathbf{r},\mathbf{r}_s). \quad (13)$$

$$U^{\mathrm{d}}(\mathbf{r},\mathbf{r}_s)=\sum_{m,n}\frac{1}{2i\beta_{mn}}\psi_{mn}(x_s,y_s)E^{\mathrm{d}}_{mn}(\mathbf{r},\mathbf{r}_s). \quad (14)$$

As also discussed in Appendix B, the direct component U^{d} corresponds physically to simple direct diffusion (1) traversing a wall with (field) transmission coefficient T at normal incidence:

$$U^{\mathrm{d}}(\mathbf{r},\mathbf{r}_s)\approx TU_{\mathrm{diff}}(\mathbf{r},\mathbf{r}_s)=\frac{Te^{-\kappa r/2}}{4\pi}\sqrt{\kappa/r+1/r^2}\xi_{\mathrm{u}}(\mathbf{r},\mathbf{r}_s) \quad (15)$$

with the range $r=|\mathbf{r}-\mathbf{r}_s|$ and $\xi_{\mathrm{u}}(\mathbf{r},\mathbf{r}_s)\sim\mathcal{CN}(0,1)$ used to represent the small scale (Rayleigh) fading.

In summary, the NLOS field z meters down the hall and d meters into the room due to a source in the hallway at $\mathbf{r}_s$ is given by

$$\begin{aligned}U_{\mathrm{room}}(\mathbf{r},\mathbf{r}_s)&=\sum_{m,n}\frac{1}{2i\beta_{mn}}\psi_{mn}(x_s,y_s)E^{\mathrm{g}}_{mn}(\mathbf{r},\mathbf{r}_s)\\&\quad+\frac{Te^{-\kappa r/2}}{4\pi}\sqrt{\kappa/r+1/r^2}\xi_{\mathrm{u}}(\mathbf{r},\mathbf{r}_s)\\&=\sum_{m,n}\psi_{mn}(x_s,y_s)\frac{e^{i\beta_{mn}|z_s|-\alpha_{mn}|z-z_s|}}{2i\beta_{mn}}A^{\mathrm{g}}_{mn}(d)\xi^{\mathrm{g}}_{mn}(\mathbf{r})\\&\quad+\frac{Te^{-\kappa r/2}}{4\pi}\sqrt{\kappa/r+1/r^2}\xi_{\mathrm{u}}(\mathbf{r},\mathbf{r}_s),\end{aligned} \quad (16)$$

where

$$E^{\mathrm{g}}_{mn}\equiv A^{\mathrm{g}}_{mn}(d)e^{i\beta_{mn}(z_s-z)-\alpha_{mn}|z-z_s|}\xi^{\mathrm{g}}_{mn}(\mathbf{r})$$

$$A^{\mathrm{g}}_{mn}(d)=\left(\frac{2m\pi}{a\sqrt{ab}}\right)\times\sqrt{\frac{T^2e^{-\kappa d}}{8k^2}\left(4\tan^{-1}(b/2d)+\pi\kappa d\ln\left(\frac{\Delta+1}{\Delta-1}\right)\right)}$$

$$\Delta=\sqrt{(2d/b)^2+1}.$$

$$\xi_{\mathrm{u}}(\mathbf{r},\mathbf{r}_s),\xi^{g}_{mn}(\mathbf{r})\sim\mathcal{CN}(0,1).$$

$$\left\langle\xi^{g}_{mn}(\mathbf{r})\xi^{g*}_{m'n'}(\mathbf{r}')\right\rangle\approx\delta_{mm'}\delta_{nn'}\delta(\mathbf{r}-\mathbf{r}'). \quad (17)$$

The dependence on hallway coordinate z_s has been factored out in the guided solution through defining a new quantity $A^{\mathrm{g}}_{mn}(d)$, independent of the hallway source coordinates. Quantities used in (17) include the hallway width a and height b, wall (field) transmission $T=0.41$ (for normal incidence on double layer interior wall, described in Appendix A), $\kappa=0.18$ nepers/m (best fit to general NLOS data in [16]), direct range $r=|\mathbf{r}-\mathbf{r}_s|$, ψ_{mn} and β_{mn} from (5) and (6). Modal loss coefficients α_{mn} and associated wall properties are discussed in Appendix A. The first (sum of guided modes) term in the field expression (16) dominates for rooms adjacent to the hallway, while the second (direct-diffusion) term dominates for rooms further from the hallway (and general NLOS conditions, as in [16]). Path gain P, defined as the ratio of received to transmit power for a small (unit gain) antennas, is related to the field U_{total}:

$$P=\lambda^2|U_{\mathrm{total}}|^2 \quad (18)$$

where λ is the wavelength. Expressions for U_{total} are given by (4) with (5) in LOS and (16) for (NLOS) hallway-room.

VI. Path Loss Predictions Compared to Measurements

Narrowband path gain measurements were collected at 2 GHz in a single hallway office building. The hallway was 3 m high and 1.65 m wide. The 35 mW transmitter was placed in the middle of a hallway, and the receive antenna was placed at different ranges both in the same hallway as well as 1 m inside various rooms along the hallway. Both antennas were vertically polarized dipoles. The receive antenna was rotated in a circle of 30 cm radius to allow for local power averaging.

Predicted path gain is compared to measurements in a single hallway office building in Fig. 2. The root mean square (rms) prediction error was found to be 1.9 dB for hallway receivers (LOS) and 3.1 dB for receivers in rooms (NLOS). Also shown is the pure diffusion model (1) path gain (through (18)), found a good match to data in general NLOS conditions [16], where hallway guidance is weak or non-existent. In a hallway that is twice as wide, the LOS signal strength was found to be some 10 dB weaker at 100 m, due to reduced guiding. This may

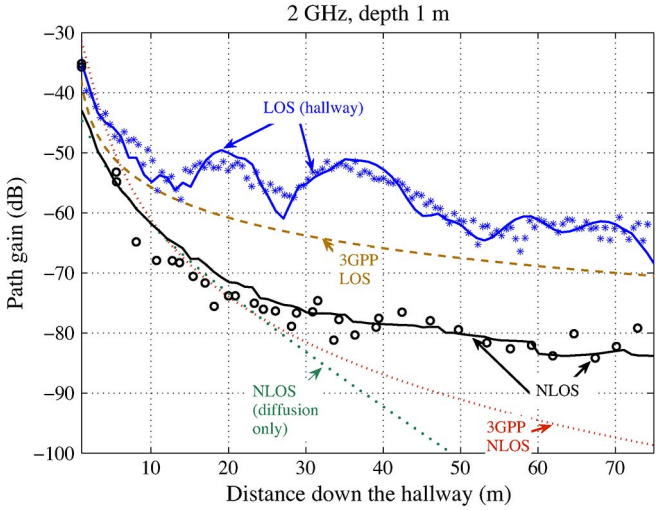

Fig. 2. Predicted and measured (both locally averaged) path gains in an office building. Transmitter is placed in the hallway, and receivers were placed either in the hallway or in rooms, as labeled. Discrete markers represent measurements, continuous curves—predictions.

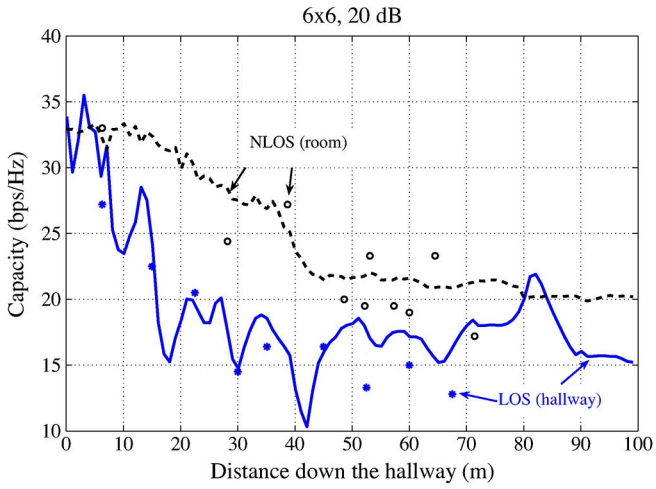

Fig. 3. Locally averaged spectral efficiency (SE) of 6×6 MIMO links vs. range for LOS and NLOS cases, evaluated at 20 dB SNR for vertical polarization. Measured values are from [25]. Note: Median SE of a 6×6 MIMO link at 20 dB SNR is 33 bps/Hz in i.i.d. channels. Discrete markers represent measurements, continuous curves—predictions.

explain correspondingly higher losses reported in the 3GPP (Winner) model [27], based on measurements that included wide corridors.

In buildings where hallway walls are less transparent, e.g., concrete or metal partition, dominant mechanism of piercing the wall may be through doors and glass panels, if present. A heuristic treatment may be done through adjusting the transmission coefficient T, say, as a sum of glass and concrete transmission coefficients, each weighted by the corresponding area fraction.

VII. MIMO Link Capacity as a Function of Range

An experimental study [25] found that MIMO capacity indoors decreases with increasing range when at least one end of the link is placed in the hallway. Since the SNR was kept constant, decreasing capacity is an indication of decreased effective scattering. Also, in [25] it was reported that correlation at the transmitter, located in the hallway of an office building, approached unit amplitude and a constant phase, regardless of whether the receive array was also in the hallway or placed inside one of the equipment-filled rooms off the hallway. At short ranges, the capacity was found to be high, both with receiver in the hallway and in a room. In this section, it is shown that the field model presented in Sections III–V is consistent with observations in [25]. The mechanism for decreasing scattering with increasing range is found to be high attenuation suffered by high-order modes, leaving only a small number of low-order modes to support the degrees of freedom.

Accordingly, the field model described above is used to evaluate theoretical (Shannon) capacity for the same antenna arrangement as in [25]. Briefly, we consider transmit and receive arrays of 6 vertically polarized antenna elements each, arranged to cover an area of about 24 cm $\times$ 24 cm. The array elements were half-wave dipole, slot antennas mounted on a large panel, thus having essentially hemispherical patterns. The transmitter array was always placed in the hallway, while the receiver array was placed either in the hallway or in a room adjacent to the hallway. In the theoretical analysis, the antenna elements were omnidirectional and arranged the same way as in the experiment. For hallway propagation, the theoretical predictions were compared against the measurements collected with transmitter and receiver arrays facing each other at various ranges. This is appropriate as the field in the hallway is dominated by low order modes, leading to a field that is directional along hallway axis. In [25], the spectral efficiency of an (open-loop) MIMO link at a fixed SNR was reported, defined, following [2], as follows:

$$C = \log_2 \left| \mathbf{I}_{N_\mathrm{T}} + \mathbf{H}_{norm}^{\dagger} \mathbf{H}_{norm} SNR/N_\mathrm{T} \right|. \qquad (19)$$

In (19) $\mathbf{I}_{N_\mathrm{T}}$ is the $N_\mathrm{T} \times N_\mathrm{T}$ identity matrix, $\|$ denotes the determinant and the normalized channel matrix $\mathbf{H}_{norm}$ is related to the actual measured channel matrix $\mathbf{H}$ through normalization by a scalar:

$$\mathbf{H}_{norm} \equiv \frac{\mathbf{H}}{\sum_{m,n} |H_{mn}|^2 \Big/ N_\mathrm{R} N_\mathrm{T}}. \qquad (20)$$

The formula (19) applies under the assumption of perfect channel knowledge at the receiver, with transmitter knowing only the rate. The spectral efficiency (19), for vertically polarized antennas at 20 dB SNR, evaluated using the LOS fields (4) and NLOS fields (16), is plotted in Fig. 3 as a function of range, along with corresponding measurements from [25]. Evaluating (19) at a fixed SNR allows a direct assessment of effective scattering, independent of absolute path loss.

It may be observed that predicted capacity is high at short ranges, where high order modes and diffuse field are both significant, providing ample scattering to support link capacity comparable to that of a Rayleigh i.i.d. channel (median of 33 bps/Hz). Link spectral efficiency when the receiver is placed in the room is generally higher, due to greater scattering richness at the receiver. With increasing range, spectral efficiency decreases significantly, by about 30% when the receiver is in the

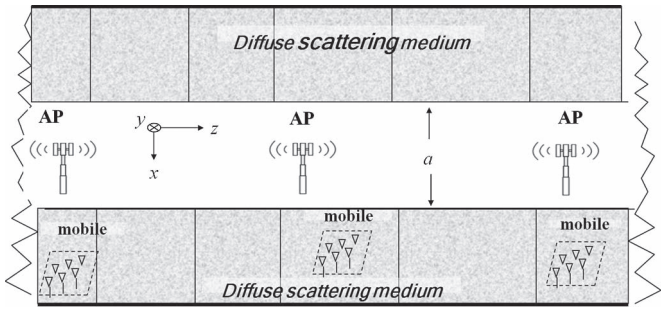

Fig. 4. Multi-cell indoor environment (top view) with APs placed in a hallway and mobiles placed in (clutter-filled) rooms.

room and about 50% when the receiver is in the hallway. This predicted behavior compares favorably to measured trends with range, as reported in Fig. 5 of [25]. It is therefore concluded that a combination of diffuse and hallway-guided fields as presented above produces predictions of both path loss and spectral efficiency that match previously reported measurements of both. This lends credibility to system simulations using this propagation model.

VIII. Capacity With Multicell Interference

The propagation model formulated above and compared against measurements in Sections VI and VII may be used in assessing a multi-cell indoor system capacity. We consider deployment of an indoor system with seven APs mounted in a line at regular spacing along a hallway, as illustrated in Fig. 4. Network edge effects are avoided through the use of the "wrap-around universe" [32]. A system simulation was conducted dropping mobiles randomly inside rooms, distributed uniformly along the z axis. Depth inside the room was fixed at 2 m (the results were only weakly dependent on depth). For each mobile, channel to each of the hallway APs was evaluated using (16) and (18), and the serving AP was identified as the one offering highest total receive power, usually the closest one. Each AP was allowed to serve only 1 mobile at a time, and mobiles were introduced until all APs were serving. Once such a set of mobiles was determined, a set of rates could be computed for the users, as described below. The procedure would be repeated again for a new set of user locations to constitute the overall statistical ensemble of rates. In what follows, user rates are compared for both open-loop and closed-loop MIMO links in the presence of full interference from all other links. These are contrasted against the rates one would expect given the common model of Rayleigh i.i.d. entries for channel matrices. In all cases, total received power was kept the same for every link (as given by the path gain model above). Since rates are generally determined by the SINR and the structure of channel matrices, normalizing the reference i.i.d. link matrices to the same power as the corresponding matrices generated from (16) illustrates the impact of the variation in degree of scattering affecting the serving and interfering signals.

We consider MIMO link rates available to a mobile placed randomly in a room (at 2 m depth), in the presence of interference from other cells. With each AP radiating a total power P_{T}

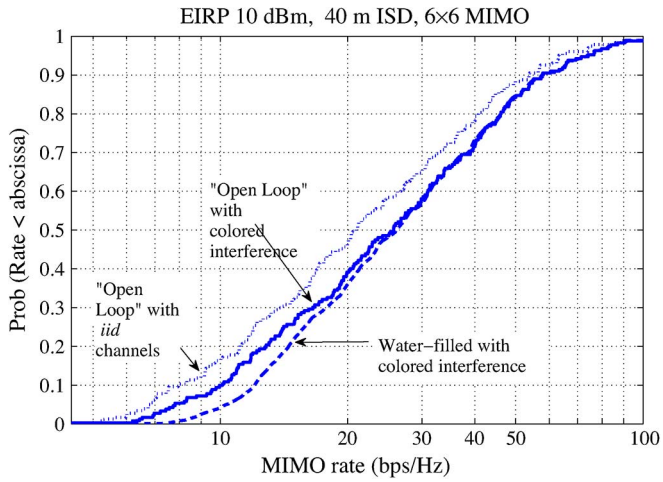

Fig. 5. Predicted rates of mutually interfering 6×6 MIMO links in an indoor network with APs arranged in a line along a hallway every 40 m. Mobiles are all inside rooms.

(10 dBm) from all of its N_{T} transmit antennas, the (generalized) open-loop Shannon rate available to a mobile in the presence of intercell interference is given by [9]:

$$C = \log_2 \left| \mathbf{I}_{N_{\mathrm{T}}} + \frac{P_{\mathrm{T}}}{N_{\mathrm{T}}} \mathbf{H}_l^{\dagger} \left(\sum_{s \neq l} \frac{P_{\mathrm{T}}}{N_{\mathrm{T}}} \mathbf{H}_s^{\dagger} \mathbf{H}_s + \mathbf{I}_{N_{\mathrm{T}}} \sigma_{\mathrm{n}}^2 \right)^{-1} \mathbf{H}_l \right|, \tag{21}$$

under the assumption of transmitter knowing only the rate, and using an identity transmit covariance. In (21), $\mathbf{H}_l$ is the MIMO channel from the serving AP, while channels from all the other APs are labeled as $\mathbf{H}_{s \neq l}$, receiver noise variance is σ_{n}^2 ($k_B T_o B$, with $B = 10$ MHz, temperature T_o and Boltzmann constant k_B) and $\mathbf{I}_{N_{\mathrm{T}}}$ is the $N_{\mathrm{T}} \times N_{\mathrm{T}}$ identity matrix. Each element of $\mathbf{H}_s$ is identified as λU, with U being the corresponding field in a room given by (16), with (17). Here, the channel coefficients are not normalized, thus including path loss. The reference case of i.i.d. distributed channel matrices is done through replacing both desired and interfering channel matrices $\mathbf{H}_s$ in (21) by spatially "white" matrices:

$$\mathbf{H}_{s,ref} \equiv \left(\sum_{m,n} |H_{s,mn}|^2 \Big/ N_{\mathrm{R}} N_{\mathrm{T}} \right)^{1/2} \mathbf{H}_{i.i.d} \tag{22}$$

where $\mathbf{H}_{i.i.d.}$ is a matrix of i.i.d. elements, each distributed as (0,1). The scalar factor in parenthesis in (22) is the average element power of the actual modeled matrix (i.e., average power gain). Using such matrices in (21) provides the reference case of channel matrices with the same power as the modeled matrices but with full scattering, while enforcing the same SINR conditions. Any difference between the full model and such a reference is then solely due to relative spatial "color" of the matrices in the full model.

Evaluating (21) for 25,000 random user locations (1 user/AP) gives a distribution of rates available to a mobile, plotted in Fig. 5, labeled as "Open-loop with colored interference". Also plotted is the distribution of rates where channel matrices are generated using a Rayleigh i.i.d. assumption, normalized to the

same effective path loss (and, thus, SINR) as the above model. These results are for the case of 40 m inter-AP separation. In this environment, the median SINR is about 12 dB.

Notably, capacities predicted using the full spatial model are higher than that using the Rayleigh i.i.d. assumption, by some 25% at the median and 15% at the 5th percentile. This may be attributed to the fact that the mobile tends to be assigned to a closer base station, which has a higher link capacity than more distant interferers, as suggested by the capacity as a function of range plots in Fig. 3. This produces interference that is more "colored" than the desired signal. Capacity formula (21) naturally takes advantage of this.

Based on the model described above, the field at large ranges is dominated by low-order modes, which have lower loss. This may be contrasted with short ranges, where the higher order modes have not yet decayed away, and diffusely scattered arrivals are still significant, resulting in a higher number of EDOF. Furthermore, for APs arranged along the hallway, total interference is primarily carried by the lower order modes, thus concentrating the interference along these common spatial dimensions, even when the user is placed in a room full of scattering objects.

The alignment of all the interfering AP's may be seen more explicitly through realizing that, at larger ranges, the direct diffuse field part of (16) may be neglected, making the total interfering field a sum of guided modes coupled into the room. Setting $z = 0$ in (16) (i.e., z-axis origin at "hotspot" center) and adding over all the interfering APs indexed by $s \neq l$ (for serving AP indexed by l), the total interfering signal for a mobile with N_{R} antennas is

$$\sum_{m,n} \begin{bmatrix} A^{\mathrm{g}}_{mn}(d)\xi^{\mathrm{g}}_{mn}(\mathbf{r}_1) \\ \vdots \\ A^{\mathrm{g}}_{mn}(d)\xi^{\mathrm{g}}_{mn}(\mathbf{r}_{N_{\mathrm{R}}}) \end{bmatrix} \times \left[\sum_{s \neq l} q_s(t)\psi_{mn}(x_s, y_s) \frac{e^{i\beta_{mn}|z_s| - \alpha_{mn}|z_s|}}{2i\beta_{mn}} \right] \quad (23)$$

where $q_s(t)$ is the information-carrying transmit signal from source s. Each modal term (indexed by m, n) in (23) is a superposition of contributions from the interfering APs in the hallway, and is manifestly a product of a source-coordinate dependent factor and a receiver-coordinate dependent factor. Each modal term is thus an outer product with a single degree of freedom [12], regardless of the number of interferers. Presence of multiple modes generally increases the total number of degrees of freedom when mode powers are comparable. Modal loss factor $e^{-\alpha_{mn}|z_s|}$ decreases monotonically with mode indices m, n (Appendix A). For large z_s, higher order modes are attenuated, leading to concentration of all interference in a few low order modes, i.e., the *same* few spatial degrees of freedom. This leaves high order modes mostly occupied by the signal from the serving base, since $z_l < z_{s \neq l}$, i.e., serving AP tends to be closer. This phenomenon is here referred to as the self-alignment of interference. While the natural mode filtering is beneficial for the dense networks studied here, it would reduce capacity for a single AP serving the entire area, as is evident from Fig. 3.

Still higher capacity may be obtained through the closed-loop MIMO procedure [9], whereby the transmit array uses the eigenmodes of the effective channel, with pre-whitened interference. Waterfilling is used to determine optimal power allocation among eigenmodes. The resulting capacity is higher than the "open-loop" capacity by about 2% at the median and 32% at 5th-percentile. Notably, such interference filtering arises naturally in this environment despite the use of only greedy single-link techniques, as opposed to active interference alignment that coordinates multiple links [26].

The disparity in the number of EDOF between the channel matrices for the desired and interfering signals depends on the inter-AP distance, as suggested by the decrease of (normalized channel) capacity with range in Fig. 3. It is found that 40 m inter-site separation in this environment results in the desired channel with a high number of EDOF and interference with a low number of EDOF. Additional numerical experiments have shown that much smaller inter-AP distances (say, 10 m) yield channels that are close to i.i.d. for both serving and interfering signals. Increasing inter-AP distance (say, to 80 m) results in channel matrices that are "colored" both for desired and interfering signals. At either extreme, the EDOF disparity is reduced. These observations are attributed solely to scattering richness variation and not to the path loss model, as assured through the use of the same path loss model in all cases. Naturally, increasing per cell capacity is not the sole metric, and total system capacity was found to increase with increasing cell density under full frequency re-use between cells.

IX. Conclusion

A three-dimensional analytical propagation theory has been developed to account for both guided and diffusely scattered fields in a generic indoor environment, containing both a LOS (hallway) and NLOS (hallway-room) propagation. Detailed building layout information is not required. The model is found to compare well to measurements of both path loss and MIMO capacity. In particular, the model reproduces the decrease of MIMO capacity with range due to a reduction in the effective number of degrees of freedom. It is found that system capacity is higher than what would be predicted using traditional range-independent models of normalized channel matrices. Interfering APs, which tend to be further, occupy channel dimensions corresponding to low order hallway modes, causing total interference to align naturally. The desired signal, originating from the nearest AP, undergoes greater scattering. The disparity in number of EDOF between signal and interference leads to higher rates that can be further improved through waterfilling applied individually to each link, based on the desired channel and the spatial covariance of the interference. The rates with waterfilling are on the order of 30% greater than would be anticipated in range-independent channel EDOF models (e.g., i.i.d.). These capacities are achieved through the use of single-user MIMO techniques, without any coordination between APs.

APPENDIX A

Modal loss may be found using the ray approximation. The sinusoidal modal field (5) may be re-written as a sum of complex exponentials, physically corresponding to two counter-propagating plane waves. Each such wave encounters the waveguide wall with a spatial period:

$$R_{x,m} = 2a\sqrt{k^2 - k_{x,m}^2}/k_{x,m}. \tag{A-1}$$

The floor or a ceiling of a waveguide of height b is encountered by the travelling wave with a spatial period

$$R_{y,n} = 2a\sqrt{k^2 - k_{y,n}^2}/k_{y,n}, \tag{A-2}$$

where the x- and y-components of the mnth-mode propagation constant are, respectively,

$$k_{x,m} = m\pi/a \quad k_{y,n} = n\pi/b. \tag{A-3}$$

The travelling wave interaction with the waveguide wall is modeled by the Fresnel plane wave reflection coefficients $V_{x,m}$ suffered every $R_{x,m}$ (A-1) meters and, for floor and ceiling $V_{y,n}$, every $R_{y,n}$ (A-2) meters. The angles of incidence (with respect to grazing) for such plane waves are $\sin^{-1}(k_{x,m}/k)$ for walls and $\sin^{-1}(k_{y,n}/k)$ for floor/ceiling.

The total loss of field strength of mnth mode after propagating a distance z down the hallway is given by

$$L_{mn}(z) = |V_{x_m}|^{\lfloor z/R_{x_m} \rfloor} |V_{y_n}|^{\lfloor z/R_{y_n} \rfloor} \tag{A-4}$$

where the number of wall strikes $\lfloor z/R_{x,m} \rfloor$ is the largest non-negative integer less than or equal to the quotient $z/R_{x,m}$, similarly defined for $z/R_{y,n}$.

The continuous modal loss approximation due to reflections from the wall, useful at large z, is

$$L_{mn}(z) \approx e^{-\alpha_{mn} z},\ \alpha_{mn} = -\ln|V_{x_m}|/R_{x_m} - \ln|V_{y_n}|/R_{y_n}. \tag{A-5}$$

The plane wave reflection coefficients $V_{x,m}$ and $V_{y,n}$ are computed for dielectric walls and concrete floor/ceiling using the standard formulae for layered media (e.g., [28]). In addition, the effect of the rough interface in scattering energy out of the coherent field was included through a field factor [29] $e^{-2(k\sigma_s \sin\theta_{\rm inc})^2}$, where σ_s is the rms surface roughness, and θ_{inc} is the modal angle of incidence (with respect to normal to the wall). To compute the reflection coefficient of the concrete ceiling, the boundary was assumed to be 20 cm thick, of complex relative dielectric permittivity (5 + 0.9i) and rms roughness of 6 cm (variation due to pipes and ducts suspended under ceiling). The interior wall separating the corridor from the rooms was modeled as two 1 cm layers of real relative dielectric constant of 3, separated by 8.5 cm of air, and rms roughness of 5 cm. The material parameters were based on recommendations in [30] and are similar to [31]. The interior wall roughness is taken to represent door frames that protrude into the hallway. The wall transmission coefficient T used in (16) was set to 0.41, as appropriate for a double-layer interior wall described above, at normal incidence. Of all the environmental parameters, it was found that the results were most sensitive to wall roughness as it was a key parameter regulating the modal decay, in turn affecting room penetration strength.

APPENDIX B

Effective modal source E_{mn} in (11) is defined through evaluating the integrals in (9), using (10) for a hallway of height b:

$$E_{mn}(\mathbf{r}, \mathbf{r}_s) = \frac{m\pi}{a}\frac{2}{\sqrt{ab}} \times \int_{-b/2}^{b/2} dy' \int_{-\infty}^{\infty} dz' U(\mathbf{r}', \mathbf{r}) \sin(n\pi y'/b) e^{i\beta_{mn}|z_s - z'|} L_{mn}. \tag{B-1}$$

The field $U(\mathbf{r}', \mathbf{r})$from a remote terminal at $\mathbf{r}$ illuminating the wall at $\mathbf{r}'$ is presumed to have gone through diffuse scattering in the room and is therefore represented as being spatially white, with zero mean and intensity given by the solution to the diffusion equation. For a source at $\mathbf{r}$, the average power flux density $\mathbf{F}_{\rm d}(r)$ [16] incident on the room wall at $\mathbf{r}'$ along the wall normal $\mathbf{n}'$ is given by the inner product:

$$\mathbf{F}_{\rm d}(r)\cdot\mathbf{n}' = \frac{e^{-\kappa r}}{(4\pi)^2}\left[\frac{\kappa}{r} + \frac{1}{r^2}\right]\hat{\mathbf{r}}\cdot\mathbf{n}' = \frac{e^{-\kappa r}}{(4\pi)^2}\left[\frac{\kappa}{r} + \frac{1}{r^2}\right]\frac{d}{r} \tag{B-2}$$

where $r = |\mathbf{r} - \mathbf{r}'|$ is the range from the mobile to a point $\mathbf{r}'$ on the wall, and d is the shortest distance ("depth") from the remote to the hallway wall. The field emerging after traversing the hallway wall of (field) transmission coefficient T is expressed statistically as a spatially white field, with a spatially varying intensity (B-2):

$$U(\mathbf{r}', \mathbf{r}) = T\frac{e^{-\kappa r/2}}{4\pi}\left(\frac{d}{r^3} + \frac{\kappa d}{r^2}\right)^{1/2}\xi(y', z'). \tag{B-3}$$

In (B-3) T is set to the magnitude of the Fresnel transmission coefficient at normal incidence (0.41 for a common interior wall, as described in Appendix A). The diffuse field fine structure (i.e., "fast fading") is modeled statistically as [17]

$$\xi(y', z') \sim \mathcal{CN}(0, 1),$$
$$\langle \xi(y', z')\xi^*(y'', z'')\rangle = \frac{\pi}{k^2}\delta(y' - y'')\delta(z' - z''). \tag{B-4}$$

Alternatively, it may be argued that the direct field illuminating the wall is stronger than the reverberation field [24], still leading to (B-3). Here, the "spatial whiteness" (B-4) of the field is induced by the non-uniform interior structure of the wall, including adjacent furniture, door jams, etc.

Using (B-3) and (B-4) in (B-1), the effective "modal" source complex amplitude E_{mn} is therefore given by

$$E_{mn} = \left\langle |E_{mn}|^2 \right\rangle^{1/2} e^{i\beta_{mn}|z_s|}\xi_{mn}(\mathbf{r}), \tag{B-5}$$

$$\langle \xi_{mn}(\mathbf{r})\xi^*_{m'n'}(\mathbf{r}')\rangle \approx \delta_{mm'}\delta_{nn'}\delta(\mathbf{r} - \mathbf{r}') \tag{B-6}$$

where the uncorrelated nature of the field is indicated by the Kronecker delta functions $\delta_{mm'}$ and $\delta_{nn'}$ for modal indices and Dirac delta function $\delta(\mathbf{r}-\mathbf{r}')$ for remote location coordinates $\mathbf{r}$. Using (A-5) for L_{mn}:

$$\left\langle |E_{mn}|^2 \right\rangle = \left(\frac{m\pi}{a}\frac{2}{\sqrt{ab}}\right)^2 \frac{T^2\pi}{4\pi k^2} \times \int_{-b/2}^{b/2} dy' \int_{-\infty}^{\infty} dz' \sin^2\left(\frac{n\pi y'}{b}\right) e^{-2\alpha_{mn}|z_s-z'|-\kappa r}\left(\frac{d}{r^3}+\frac{\kappa d}{r^2}\right) \tag{B-7}$$

Here, $r=|\mathbf{r}-\mathbf{r}'|=\sqrt{d^2+y'^2+(z'-z)^2}$ is the range from the room antenna to the integration point on the hallway wall. The approximation (B-6) is justified when considering (B-1), (B-3), and (B-4), with intensity (B-3) having larger characteristic spatial scale than hallway mode functions.

Significant contributions to (B-7) arise from two generally distinct regions, near $z'=z$ and $|z_s-z'|=0$. Respectively, these are locations to which either the diffuse/spreading losses in the room are minimized or where the hallway modal propagation losses minimized. These regions coalesce into one near $|z_s-z|=0$. Neglecting this special case for simplicity, the integrand in (B-7) is viewed as consisting of two factors, each highly peaked in its own region of z' and approximately constant near the peak of the other factor. In all cases, $\sin^2(n\pi y'/b)$ will be approximated as 1/2, justified by recognizing that other factors in the integrand vary with y' much slower than $\sin(2n\pi y'/b)$.

Accordingly, the first contribution to the integral is evaluated by setting $e^{-2\alpha_{mn}|z_s-z'|}\approx e^{-2\alpha_{mn}|z_s-z|}$ near $z'=z$:

$$\begin{aligned}\left\langle |E^{\mathrm{g}}_{mn}|^2 \right\rangle &= \frac{1}{8\pi k^2}\left(\frac{2m\pi}{a\sqrt{ab}}\right)^2 T^2\pi e^{-2\alpha_{mn}|z_s-z|}e^{-\kappa d}d \\ &\quad\times \int_{-b/2}^{b/2} dy' \int_{-\infty}^{\infty} dz' \left(\frac{1}{r^3}+\frac{\kappa}{r^2}\right) \\ &= \left(\frac{2m\pi}{a\sqrt{ab}}\right)^2 \frac{T^2 e^{-2\alpha_{mn}|z_s-z|}de^{-\kappa d}}{8k^2} \\ &\quad\times \int_{-b/2}^{b/2} dy' \left(\frac{2}{d^2+y'^2}+\frac{\pi\kappa}{\sqrt{d^2+y'^2}}\right).\end{aligned} \tag{B-8}$$

Leading to

$$\left\langle |E^{\mathrm{g}}_{mn}|^2 \right\rangle = \left(\frac{2m\pi}{a\sqrt{ab}}\right)^2 \frac{T^2 e^{-2\alpha_{mn}|z_s-z|}e^{-\kappa d}}{8k^2} \times \left(4\tan^{-1}(b/2d)+\pi\kappa d\ln\left(\frac{\sqrt{(2d/b)^2+1}+1}{\sqrt{(2d/b)^2+1}-1}\right)\right). \tag{B-9}$$

It may be recognized that this expression corresponds to guided modal contributions (thus the superscript 'g') that reach the region in the hallway nearest the remote antenna, and then undergoes diffuse scattering/spreading to reach the remote antenna.

Another contribution to (B-7) is evaluated in the vicinity of $|z_s-z'|=0$, where $r\approx\sqrt{r_{\mathrm{h}}^2+y'^2}$, defined in terms of the horizontal range $r_{\mathrm{h}}\equiv\sqrt{d^2+\bar{z}^2}$ and $\bar{z}\equiv z_s-z$:

$$\begin{aligned}\left\langle \left|E^{\mathrm{d}}_{mn}\right|^2 \right\rangle &\approx \left(\frac{2m\pi}{a\sqrt{ab}}\right)^2 \frac{T^2 e^{-\kappa r_{\mathrm{h}}}}{8k^2}\int_{-\infty}^{\infty} dz' e^{-2\alpha_{mn}|z_s-z'|} \\ &\quad\times \int_{-b/2}^{b/2} dy' \left(\frac{d}{\left(r_{\mathrm{h}}^2+y'^2\right)^{3/2}}+\frac{\kappa d}{\left(r_{\mathrm{h}}^2+y'^2\right)}\right) \\ &= \left(\frac{2m\pi}{a\sqrt{ab}}\right)^2 \frac{T^2 e^{-\kappa r_{\mathrm{h}}}d}{8k^2\alpha_{mn}r_{\mathrm{h}}^2} \\ &\quad\times \left(\frac{b}{\sqrt{r_{\mathrm{h}}^2+(b/2)^2}}+2\kappa r_{\mathrm{h}}\tan^{-1}\left(\frac{b}{2r_{\mathrm{h}}}\right)\right).\end{aligned} \tag{B-10}$$

For most locations $b/2 \ll r_{\mathrm{h}}$, and (B-10) simplifies to

$$\left\langle \left|E^{\mathrm{d}}_{mn}\right|^2 \right\rangle \approx \left(\frac{2m\pi}{a\sqrt{ab}}\right)^2 \frac{T^2 bde^{-\kappa r_{\mathrm{h}}}}{8k^2\alpha_{mn}}\left(\frac{1}{r_{\mathrm{h}}^3}+\frac{\kappa}{r_{\mathrm{h}}^2}\right). \tag{B-11}$$

The form of (B-11) suggests a physical interpretation: this component is due to the field from the hallway source illuminating the wall near the source, from where the signal undergoes direct (thus the superscript 'd') diffusion/spreading to the remote.

The total modal coupling coefficient is therefore a sum of the guided and direct components:

$$E_{mn}\approx E^{\mathrm{g}}_{mn}+E^{\mathrm{d}}_{mn}. \tag{B-12}$$

$$E^{\mathrm{g}}_{mn}\equiv\left\langle |E^{\mathrm{g}}_{mn}|^2\right\rangle^{1/2} e^{i\beta_{mn}(z_s-z)}\xi^{\mathrm{g}}_{mn}. \tag{B-13}$$

$$E^{\mathrm{d}}_{mn}\equiv\left\langle \left|E^{\mathrm{d}}_{mn}\right|^2\right\rangle^{1/2} \xi^{\mathrm{d}}_{mn}. \tag{B-14}$$

Here, $\langle \xi^{\mathrm{g}}_{mn}{\xi^{\mathrm{d}}_{mn}}^{*}\rangle=0$, since different scatterers are generally involved in these two diffuse components.

The direct diffusion component E^{d}_{mn} in (B-14) and (B12) is the modal representation of simple diffusion, where the hallway source directly illuminating the closest part of the hallway wall with high-order modes contributing most significantly to (11). In this region, the modal representation of a field in waveguide with penetrable walls is least accurate. A simple alternative followed here is to replace the modal sum for the direct diffusion component with the homogeneous diffuse field U_{diff}, based on (1), attenuated by the wall transmission coefficient T.

REFERENCES

[1] G. J. Foschini, "Layered space-time architecture for wireless communication in a fading environment when using multiple antennas," *Bell Labs Tech. J.*, vol. 1, no. 2, pp. 41–59, Autumn, 1996.

[2] G. J. Foschini and M. Gans, "On the limits of wireless communications in a fading environment when using multiple antennas," *Wireless Pers. Commun.*, vol. 6, no. 6, pp. 311–335, Mar. 1998.

[3] T. L. Marzetta, "How much training is required for multiuser MIMO?" in *Proc. 40th Asilomar Conf. Signals, Syst. Comput.*, Oct./Nov. 2006, pp. 359–363.

[4] L. Zheng and D. N. C. Tse, "Communication on the Grassmann manifold: A geometric approach to the noncoherent multiple-antenna channel," *IEEE Trans. Inf. Theory*, vol. 48, no. 2, pp. 359–383, Feb. 2002.

[5] D. Chizhik *et al.*, "Multiple-input–multiple-output measurements and modeling in Manhattan," *IEEE J. Sel. Areas Commun.*, vol. 21, no. 3, pp. 321–331, Apr. 2003.

[6] Y. Kai *et al.*, "A wideband statistical model for NLOS indoor MIMO channels," in *Proc. IEEE 55th VTC-Spring*, 2002, vol. 1, pp. 370–374.

[7] "Technical specification group radio access network; evolved universal terrestrial radio access (E-UTRA); Further advancements for E-UTRA physical layer aspects, (Release 9)," Sophia-Antipolis Cedex, France, TR 36.814 V9.0.0 (2010-03), 2010. [Online]. Available: ftp://ftp.3gpp.org/Specs/archive/36_series/36.814

[8] 1ST-WINNER II Deliverable J.J.2 v. l.2., "WINNER II Channel Models," 1ST-WINNER II. Tech. Rep., 2007. [Online]. Available: http://www.istwinner.corg/deliverables.html

[9] F. R. Farrokhi, G. J. Foschini, A. Lozano, and R. A. Valenzuela, "Link-optimal space-time processing with multiple transmit and receive antennas," *IEEE Commun. Lett.*, vol. 5, no. 3, pp. 85–87, Mar. 2001.

[10] G. Caire and S. Shamai, "On the achievable throughput of a multiantenna Gaussian broadcast channel," *IEEE Trans. Inf. Theory*, vol. 49, no. 7, pp. 1691–1706, Jul. 2003.

[11] H. Huang *et al.*, "Increasing downlink cellular throughput with limited network MIMO coordination," *IEEE Trans. Wireless Commun.*, vol. 8, no. 6, pp. 2983–2989, Jun. 2009.

[12] D. Chizhik, G. J. Foschini, M. J. Gans, and R. A. Valenzuela, "Keyholes, correlations, capacities of multielement transmit and receive antennas," *IEEE Trans. Wireless Commun.*, vol. 1, no. 2, pp. 361–368, Apr. 2002.

[13] D. Gesbert, H. Bolcskei, D. A. Gore, and A. J. Paulraj, "Outdoor MIMO wireless channels: Models and performance prediction," *IEEE Trans. Commun.*, vol. 50, no. 12, pp. 1926–1934, Dec. 2002.

[14] A. Ishimaru, *Wave Propagation and Scattering in Random Media*. Piscataway, NJ, USA: IEEE Press, 1997, ser. Series on Electromagnetic Wave Theory.

[15] D. Ullmo and H. U. Baranger, "Wireless propagation in buildings: A statistical scattering approach," *IEEE Trans. Veh. Technol.*, vol. 48, no. 3, pp. 947–955, May 1999.

[16] D. Chizhik, J. Ling, and R. A. Valenzuela, "Radio wave diffusion indoors and throughput scaling with cell density," *IEEE Trans. Wireless Commun.*, vol. 11, no. 9, pp. 3284–3291, Sep. 2012.

[17] M. J. Beran and G. B. Parrent, *Theory of Partial Coherence*. Englewood Cliffs, NJ, USA: Prentice-Hall, 1964.

[18] C. A. Balanis, *Advanced Engineering Electromagnetics*. Hoboken, NJ, USA: Wiley, 1989.

[19] N. Yarkony and N. Blaunstein, "Prediction of propagation characteristics in indoor radio communication environments," in *Proc. EuCAP*, Nov. 2007, pp. 151–174.

[20] D. Porrat and D. C. Cox, "UHF propagation in indoor hallways," *IEEE Trans. Wireless Commun.*, vol. 3, no. 4, pp. 1188–1198, Jul. 2004.

[21] D. Porrat, P. Kyritsi, and D. C. Cox, "MIMO capacity in hallways and adjacent rooms," in *Proc. IEEE GLOBECOM*, Nov. 17–21, 2002, vol. 2, pp. 1930–1934.

[22] P. Kyritsi, D. C. Cox, R. A. Valenzuela, and P. W. Wolniansky, "Effect of antenna polarization on the capacity of a multiple element system in an indoor environment," *IEEE J. Sel. Areas Commun.*, vol. 20, no. 6, pp. 1227–1239, Aug. 2002.

[23] A. Ishimaru, *Electromagnetic Wave Propagation, Radiation, Scattering*. Englewood Cliffs, NJ, USA: Prentice-Hall, 1990.

[24] J. B. Andersen, J. O. Nielsen, G. F. Pedersen, G. Bauch, and M. Herdin, "Room electromagnetics," *IEEE Antennas Propag. Mag.*, vol. 49, no. 2, pp. 27–33, Apr. 2007.

[25] P. Kyritsi, D. C. Cox, R. A. Valenzuela, and P. W. Wolniansky, "Correlation analysis based on MIMO channel measurements in an indoor environment," *IEEE J. Sel. Areas Commun.*, vol. 21, no. 5, pp. 713–720, Jun. 2003.

[26] V. R. Cadambe and S. A. Jafar, "Interference alignment and degrees of freedom of the K-user interference channel," *IEEE Trans. Inf. Theory*, vol. 54, no. 8, pp. 3425–3441, Aug. 2008.

[27] WINNER II Channel Models, IST-4-027756 WINNER II, D1.1.2 V1.2, 2007.

[28] M. Born and E. Wolf, *Principles of Optics*. Cambridge, U.K.: Cambridge Univ. Press, 1997.

[29] P. Beckmann and A. J. Spizzichino, *The Scattering of Electromagnetic Waves From Rough Surfaces*. Norwood, MA, USA: Artech, 1987.

[30] M. D. Baker-Jarvis *et al.*, "Measuring the permittivity and permeability of lossy materials: Solids, liquids, metals, building materials, negative-index materials," Nat. Inst. Sci. Technol., Boulder, CO, USA, NIST Tech. Note 1536, 2005.

[31] "Digital mobile radio towards future generation systems, final report," Brussels, Belgium, Tech. Rep. COST Action 231, 1999.

[32] H. C. Huang, C. B. Papadias, and S. Venkatesan, *MIMO Communication for Cellular Networks*. New York, NY, USA: Springer-Verlag, 2011.

[33] D.-S. Shiu, G. J. Foschini, M. J. Gans, and J. M. Kahn, "Fading correlation and its effect on the capacity of multielement antenna systems," *IEEE Trans. Commun.*, vol. 48, no. 3, pp. 502–513, Mar. 2000.

[34] H. Xia, H. L. Bertoni, L. R. Maciel, A. Lindsay-Stewart, and R. Rowe, "Radio propagation characteristics for line-of-sight microcellular and personal communications," *IEEE Trans. Antennas Propag.*, vol. 41, no. 10, pp. 1439–1447, Oct. 1993.

Dmitry Chizhik (F'14) received the Ph.D. degree in electrophysics from Polytechnic University, Brooklyn, NY, USA. His thesis work has been in ultrasonics and non-destructive evaluation. He joined the Naval Undersea Warfare Center, New London, CT, USA, where he did research in scattering from ocean floor, geoacoustic modeling of porous media and shallow water acoustic propagation. In 1996, he joined Bell Laboratories, working on radio propagation modeling and measurements, using deterministic and statistical techniques. He has worked on measurement, modeling and channel estimation of MIMO channels. The results are used both for determination of channel-imposed bounds on channel capacity, system performance and for optimal antenna array design. His recent work has included system and link simulations of satellite and femto cell radio communications that included all aspects of the physical layer. His research interests are in acoustic and electromagnetic wave propagation, signal processing, communications, radar, sonar, and medical imaging. He a recipient of the Bell Labs President's Award.

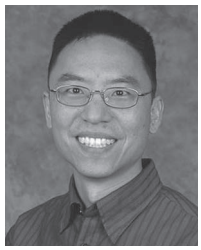

Jonathan Ling received the B.Sc. degree in electrical engineering from Rutgers University, Piscataway, NJ, USA, and the M.Sc. degree in computer science and the Ph.D. degree in electrical engineering from Stevens Institute, Hoboken, NJ, USA. He joined the Wireless Communications Research Department, Bell Laboratories, Holmdel, NJ, USA, in 1994. He has conducted multiple-input–multiple-output radio propagation measurements and modeling and helped develop the WiSE ray-tracing tool. His research interests are media access, wireless systems, channel modeling, and signal processing.

Reinaldo A. Valenzuela (F'99) received the B.Sc. degree from the University of Chile and the Ph.D. degree from Imperial College. He is the Director of the Wireless Communications Research Department and a Distinguished Member of the Technical Staff of Bell Laboratories. He has been engaged in multiple-input–multiple-output/space time systems achieving high capacities using transmit and receive antenna arrays. He has published over 189 papers and is a holder of 44 patents. He has over 20 000 Google Scholar citations and is a "Highly Cited Author" in Thomson ISI. He is a Fulbright Senior Specialist. He was a recipient of the 2010 IEEE Eric E. Sumner Award and is a Fellow of Bell Labs and WWRF.